

Reversible Data Hiding with Difference Prediction and Content Characteristics

Feng-Cheng Chang

Department of Innovative Information and Technology, Tamkang University
180 Linwei Road, Jiaosi, Ilan 262, Taiwan, R.O.C.
135170@mail.tku.edu.tw

Hsiang-Cheh Huang*

Department of Electrical Engineering, National University of Kaohsiung
700 University Road, Kaohsiung 811, Taiwan, R.O.C.

*Corresponding author.
hch.nuk@gmail.com

Received August, 2015; revised December, 2015

ABSTRACT. *In this paper, we propose a new algorithm in reversible data hiding, with the applications of privacy protection for digital images. Information security has long been an important topic in research and practical applications, and reversible data hiding has attracted more and more attention recently. In order to look for better performances, unlike conventional schemes, we employ the difference between original and predicted images for hiding secret information at the encoder. We take the inherent characteristics of original image into account, and we employ prediction techniques to produce predicted image. With the alteration of difference histogram, acquired between predicted and original images, more amount of capacity for data embedding can be reached with similar output image quality in reversible data hiding. At the decoder, with the small amount of side information, both the original image and secret information can be extracted. This implies the reversibility of proposed algorithm. In addition, extracted secret information is authenticated to retain the ownership. Simulation results demonstrate the superiority over existing schemes, and the effectiveness for practical applications with digital images.*

Keywords: Reversible data hiding, Difference histogram, Prediction, Authentication.

1. Introduction. Data hiding is one of the important schemes for digital rights management (DRM) and information security [1, 2], including content authentication and copyright protection [3, 4]. User defined secret information, or watermark, is embedded into original multimedia contents, images for instance, and marked image is delivered to the receiver. Conventional watermarking techniques aim at examining authenticity between embedded watermark and extracted one. Under this scenario, at the encoder, the watermark is embedded, which causes irreversible degradation of original image can be expected. At the receiver, the watermark embedded beforehand is extracted, and it is compared to the embedded one to examine the authenticity. Only the extracted watermark should be examined, and the marked image is ignored [5, 6].

The concepts of reversible data hiding have emerged in early 2000's [7, 8, 9]. Similar to its watermarking counterpart, at the encoder, secret information is embedded into images

by algorithms developed by researchers. At the receiver, unlike conventional watermarking, not only the embedded watermark should be extracted, but the original image should also be recovered. More importantly, the extracted watermark and the recovered image should be identical to their counterparts at the encoder, and this is the origin of the term ‘reversible data hiding’ comes from [10, 11, 12]. With these requirements, practical implementations for reversible data hiding can roughly be classified into two categories, one is to alter the relationships among neighboring pixels from the standpoint of spatial locality [13, 14, 15, 16], and the other is to modify the histogram of original image from the global point of view [17, 18, 19, 20]. With the integration of the two categories, difference histograms can be utilized to reach enhanced performances.

There are parameters to assess the performances of reversible data hiding algorithms [15, 20], including reversibility, embedding capacity, marked image quality, and side information for decoding. First, reversibility refers to the capability to make reversible data hiding possible. That is, at the decoder, with reasonable amount of side information, both the secret information and the original image should be perfectly recovered. Second, the more amount of embedding capacity adds the flexibility for algorithm designers to embed the secret information. Next, the marked image and the original one should look alike, or the distortion induced should be as small as possible. Finally, the side information denotes the reasonable amount of auxiliary information, which is expected to be few, for the decoder to make the recovery of original image and embedded secret possible.

In this paper, we focus on reversible data hiding with prediction-based techniques. Different from conventional techniques, predicted image is generated from original one in advance, and difference values between the two are utilized for data hiding. The histogram of difference values is generated, and intentional alteration of the histogram, where no calculation is needed, can make reversible data hiding possible. With the evaluation criteria offered, simulation results exhibit better performances over existing algorithms.

This paper is organized as follows. In Sec. 2, we discuss about conventional algorithms in reversible data hiding. In Sec. 3 we then describe the proposed algorithm based on prediction techniques. Experimental results are demonstrated in Sec. 4. Finally, we conclude this paper in Sec. 5.

2. Conventional Schemes. It has long been an effective means to utilize characteristics of original images for data hiding [21, 22]. We can classify conventional schemes into two categories, one is by modifying the difference value between neighboring pixels [13, 14, 15, 16], and the other is by altering the histogram of original image [17, 18, 19, 20]. For the former category, it takes the local characteristics into account, and for the latter one, it considers the slightest modification of global statistics of original image.

On the one hand, the difference expansion (DE) method is one of the earliest schemes for reversible data hiding [13, 14, 15, 16]. It follows the concepts from wavelet transforms. Two neighboring pixels in the original image are selected. The average, referring to the low-frequency component, is kept the same, and the difference between the two, referring to the high-frequency component, is intentionally doubled, and then the secret bit is added to complete the data hiding procedure. By employing the inverse wavelet transform between the low- and modified high-frequency components, marked image can be reconstructed. Occasionally, overflow in some pairs may occur, and these locations should be recorded into the ‘location map’, or the side information for data extraction, for keeping the reversibility of the algorithm [16, 23].

The DE-based scheme is famous for the high capacity for data embedding. For legitimate pairs, one bit can be embedded into two bytes, leading to the embedding capacity of

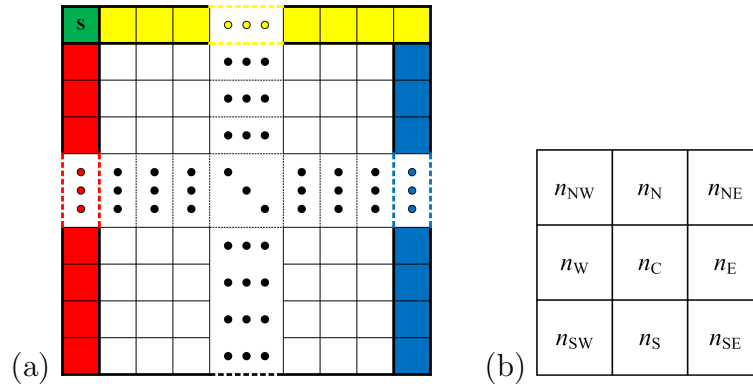


FIGURE 1. Formation of predicted image. (a) Five types of classifications, denoted by different colors, in the original $M \times N$ image. (b) Weighting factors for data prediction.

0.5 bit/pixel (bpp). However, for pairs unsuitable for embedding, the size of location map, containing coordinate of unsuitable pairs, should be deducted from embedding capacity.

On the other hand, the histogram-based method [17, 18, 19, 20] is famous for its ease of implementation and few overhead generated. Histogram of original image is generated, and two parameters for reversible data hiding are determined first. Within the histogram, the luminance value corresponding to the maximal occurrence is called the peak point, and the first luminance value with no occurrence, which is larger than that of the peak point, is named the zero point. The portion between peak and zero points are intentionally altered to make data embedding possible. With this kind of method, capacity is limited by the number of maximal occurrence, which is the major drawback. On the contrary, very few side information, only two bytes for representing luminance values of peak and zero points, is necessary.

Luminance values tend to be similar between neighboring pixels are similar for ordinary images [21, 22]. By taking difference values and producing corresponding histogram [24], conventional histogram-based method can be utilized for data hiding, while the increased capacity can be expected. Besides, ideas from difference expansion can also be applied. By following this concept, new data hiding scheme can be proposed in Sec. 3.

3. Proposed Algorithm. By modifying the difference values, high embedding capacity can be reached, while considerable amount of side information may also be needed for decoding. From another perspective, by utilizing the histogram, simple operation would be desirable, while limited embedding capacity is the major drawback. Thus, considering advantages of the two types of techniques, algorithms with better performances can be derived. Besides producing difference values from original image alone, we generate the predicted image first, calculate the differences between predicted and original images, and perform data embedding by altering the difference values with the concept of DE-based schemes. By doing so, our method meets considerable increase in embedding capacity, and comparable quality in marked image, along with reduced size in side information.

Here we describe the prediction-based reversible data hiding algorithm in this paper, with the concept in [24]. Data embedding procedures are described as follows.

1. Generate the predicted image. We take the image \mathbf{X} with the size of $M \times N$ in the original image as an instance in Fig. 1(a). Predicted image to be produced subsequently is denoted by \mathbf{X}_p . Prediction of data starts from the pixel at upper-left corner, or $X(0, 0)$, as the seed, denoted by ‘S’ in green color. Next, luminance

prediction of the pixels in the first row, shown in yellow, is determined with Eq. (1).

$$X_p(0, j) = X(0, j - 1), \quad j = 1, \dots, N - 1. \quad (1)$$

Then, luminance prediction of the pixels in the first column, shown in red, is calculated based on the weighting factors in Fig. 1(b). The subscript ‘c’ at the center implies the current position, and subscripts surrounding the current position denote the directions to corresponding factors.

$$X_p(i, 0) = \text{round} \left(\frac{n_N X(i - 1, 0) + n_{NE} X(i - 1, 1)}{n_N + n_{NE}} \right), \quad i = 1, \dots, M - 1. \quad (2)$$

Luminance prediction of pixels in the last column, shown in blue, is calculated.

$$X_p(i, N-1) = \begin{cases} \min(X(i-1, N-1), X(i, N-2)), & X(i, N-1) \geq \max(X(i-1, N-1), X(i, N-2)); \\ \max(X(i-1, N-1), X(i, N-2)), & X(i, N-1) \leq \min(X(i-1, N-1), X(i, N-2)); \\ X(i-1, N-1) + X(i, N-2) - X(i-1, N-2), & \text{otherwise.} \end{cases} \quad (3)$$

For remaining pixels shown in white, predicted pixels can be calculated with pixels in the upper-left (northwest), upper (north), upper-right (northeast), and left (west), with the properly selected weighting factors

$$X_p(i, j) = \text{round} \left(\frac{n_{NW} X(i - 1, j - 1) + n_N X(i - 1, j) + n_{NE} X(i - 1, j + 1) + n_W X(i, j - 1)}{n_{NW} + n_N + n_{NE} + n_W} \right). \quad (4)$$

With Eqs. (2) and (4), by following raster scanning, we are going to adjust factors of n_{NW} , n_N , n_{NE} , and n_W in Fig. 1(b) for obtaining the larger capacity with the better output image quality.

2. After prediction, differences between original and predicted images are calculated by

$$d(i, j) = X_p(i, j) - X(i, j). \quad (5)$$

The difference histogram $d(i, j)$, denoted by an array $D(k)$, $-255 \leq k \leq 255$, is generated. From the concepts of DE-based schemes and histogram-based techniques, we can perform reversible data hiding for obtaining the advantages from both techniques with the alteration of difference histogram in Eq. (5).

3. We set the positive-integer-valued embedding level, EL, and the embedding round index, $r_{em} = \lfloor \frac{EL}{2} \rfloor$, where $\lfloor \cdot \rfloor$ denotes the floor function, for data embedding. EL means the number of bins in difference histogram around 0, and r_{em} operates as separator between positive and negative values.

Data embedding schemes for odd- and even-valued EL are a bit different. For odd-valued EL, if EL=3, then $r_{em}=1$, we take $-1, 0$, and 1 in the difference histogram for data embedding. The sum of heights of the three bins implies the embedding capacity. For even-valued EL, if EL=4, then $r_{em}=2$, we take $-1, 0, 1$, and 2 . Again, the sum of heights of the four bins implies the embedding capacity. Larger EL values bring about larger embedding capacity, because more bins can be altered for embedding. Then, more modifications to difference values can be expected, and larger degradation to output image. Additionally, larger EL values may cause the increase in side information, because difference values at extremes may be moved to lie outside the range between -255 and 255 . Locations correspond to such kind of difference values should be recorded as ‘location map’ for decoding [15, 23].

The odd- or even-valued r_{em} also influences the data embedding procedure. For odd-valued EL, the difference histogram $D(k)$ is modified to $\tilde{D}(k)$, and some spaces are intentionally left blank for data embedding.

$$\tilde{D}(k) = \begin{cases} D(k) + r_{em}, & \text{if } D(k) > r_{em}; \\ D(k) - r_{em} - 1, & \text{if } D(k) < -r_{em}; \\ D(k), & \text{otherwise.} \end{cases} \quad (6)$$

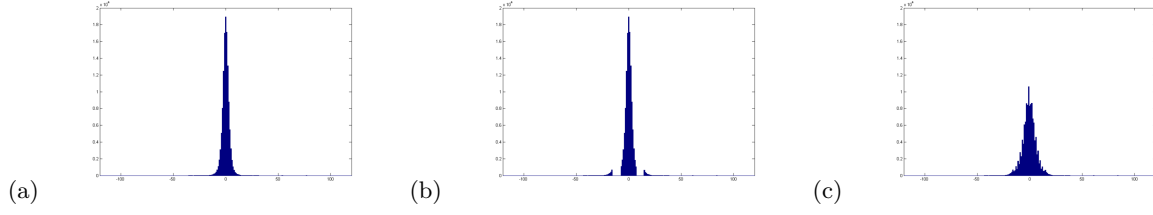


FIGURE 2. Comparisons of difference histograms. (a) Original difference histogram. (b) Emptying regions between -7 and 7 in Fig. 2(a) for $EL=15$. (c) Difference histogram after data embedding.

For even-valued EL ,

$$\tilde{D}(k) = \begin{cases} D(k) + r_{em}, & \text{if } D(k) > r_{em}; \\ D(k) - r_{em}, & \text{if } D(k) < -r_{em} + 1; \\ D(k), & \text{otherwise.} \end{cases} \quad (7)$$

4. Suppose the difference values after embedding the secret data bit, w , can be denoted by $D'(k)$. For an odd-valued r_{em} , if $r_{em} \geq 1$, data embedding is performed by

$$D'(k) = \begin{cases} \tilde{D}(k) + r_{em} - 1 + w, & \text{if } \tilde{D}(k) = r_{em}; \\ \tilde{D}(k) - r_{em} - w, & \text{if } \tilde{D}(k) = -r_{em}; \\ \tilde{D}(k), & \text{otherwise.} \end{cases} \quad (8)$$

Next, r_{em} is decreased by 1 iteratively. After performing Eq. (8) recursively until $r_{em} = 0$, data embedding is performed by

$$D'(k) = \begin{cases} \tilde{D}(k) - w, & \text{if } \tilde{D}(k) = r_{em}; \\ \tilde{D}(k), & \text{otherwise.} \end{cases} \quad (9)$$

On the other hand, for an even-valued r_{em} ,

$$D'(k) = \begin{cases} \tilde{D}(k) + r_{em} - 1 + w, & \text{if } \tilde{D}(k) = r_{em}; \\ \tilde{D}(k) - r_{em} - 1 - w, & \text{if } \tilde{D}(k) = -r_{em} + 1; \\ \tilde{D}(k), & \text{otherwise.} \end{cases} \quad (10)$$

Eq. (10) is executed recursively until $r_{em} = 0$.

5. Reconstruct the output image by adding the difference value back to the predicted image. By using raster scan, the modified difference value after data embedding, $D'(k)$, can be turned into $d'(i, j)$, and marked image $X_w(i, j)$ is obtained by

$$X_w(i, j) = X_p(i, j) - d'(i, j). \quad (11)$$

Here we provide a simple illustration to the notations in Eqs. (5) to (10) in Fig. 2, with the **Lena** test image with size 512×512 as the original. We use the weighting factors of $(n_{NW}, n_N, n_{NE}, n_W) = (1, 8, 7, 8)$ for producing predicted image. After calculating the difference between predicted and original image in Eq. (5), histogram of $D(k)$ is depicted in Fig. 2(a). Next, in Fig. 2(b), we set $EL = 15$, and then $r_{em} = \lfloor \frac{15}{2} \rfloor = 7$. It implies that difference values between -7 and 7 are ready for data embedding. Finally, with calculations in Eqs. (6), (8), and (9), the modified difference after data embedding is presented in Fig. 2(c). We need to note that the maximum values of vertical axis in Figs. 2(a), (b), and (c) are identical, and we can easily tell the differences in shape among the three difference histograms before and after data embedding.

Extraction of secret data and recovery of original image are the reverse procedures to the embedding counterpart. At the beginning, the secret data and original image should be extracted from the marked image $X_w(i, j)$, and the embedding level, EL , and weighting factors of n_{NW} , n_N , n_{NE} , and n_W , should be received at the decoder as side information. Pixels at the first column in Fig. 1(a) are recovered first based on Eq. (2), then the first

TABLE 1. Comparisons of maximal embedding capacity and their PSNR, EL, and parameters for six test images with sizes of 512×512 .

Image	Capacity (bpp)	Quality (dB)	EL	$(n_{NW}, n_N, n_{NE}, n_W)$
aerial	0.5291	31.13	18	(1, 4, 2, 7)
APC	0.9444	33.87	25	(1, 3, 2, 8)
Barbara	0.6983	32.93	18	(1, 8, 3, 1)
F16	0.9326	33.56	30	(1, 3, 4, 8)
Goldhill	0.8950	31.44	28	(1, 8, 3, 8)
Lena	0.9347	34.32	25	(1, 8, 7, 8)

row and the last column are predicted by Eqs. (1) and (3), respectively, and finally, the rest of the pixels are calculated with Eq. (4). Difference values are then produced. With EL, secret bits can be retrieved. By following procedures in reverse order, original image and hidden secret can be separated and both can be recovered perfectly.

In comparison with conventional histogram-based scheme [17, 18, 19, 20], or difference expansion (DE) scheme [13, 14, 15, 16], the amount of side information is relatively fewer than its corresponding counterparts, because only the four weighting factors and the EL value are required for decoding. Considering practical applications, the EL values may be carefully selected to prevent the overflow of difference values, and hence there is no need to produce the location map. From the derivations and discussions above, proposed method combine the advantages from both the histogram-based and DE-based schemes in reversible data hiding. Simulations results in Sec. 4 also support this standpoint.

4. Simulation Results. We have conducted experiments with six test images to examine the effectiveness of proposed algorithm. Performances with relating algorithm in [24] are also compared. Both output image quality and embedding capacity are observed.

In Eqs. (1) to (4), the four parameters for image prediction, n_{NW} , n_N , n_{NE} , and n_W , are trained in advance based on minimization of squared error between original and predicted images with our algorithm. Therefore, the differences between predicted and original images, $d(i, j)$, tend to be small, implying high peaks around zero in the difference histogram $D(k)$. With this derivation, larger capacities with our algorithm can be obtained. Considering practical implementations, we set these four weighting parameters to be integer values between 1 and 16. After training, suitable parameter values are $(n_{NW}, n_N, n_{NE}, n_W) = (1, 8, 7, 8)$ for **Lena** test image for instance, and parameter values correspond to other test images, including **aerial**, **APC**, **Barbara**, **F16**, and **Goldhill**, are represented in Table 1. Next, the difference values can be produced in Eq. (5), and with the provided embedding level, EL, data can be embedded subsequently with Eqs. (6) to (11). Besides, in [24], four parameters for all the test images are fixed to be $(n_{NW}, n_N, n_{NE}, n_W) = (1, 2, 1, 2)$, which may lead to the inferior performance for data hiding. Inherent characteristics of test images should be different, and hence one test image should meet the different values of weighting parameters, as depicted in Table 1. Besides, the maximal embedding capacity, along with output image quality and EL values, are also displayed in Table 1. Here, capacity is measured by bit per pixel (bpp), or the number of secret bits that can be hidden into the number of pixels in the original image. Marked image quality is assessed by peak signal-to-noise ratio (PSNR). Again, EL means the number of bins in difference histogram around 0, as we mentioned in Sec. 3.

Regarding to the amount of side information, with [24], the four parameters, along with the embedding level EL, are served as the side information for decoding. For our

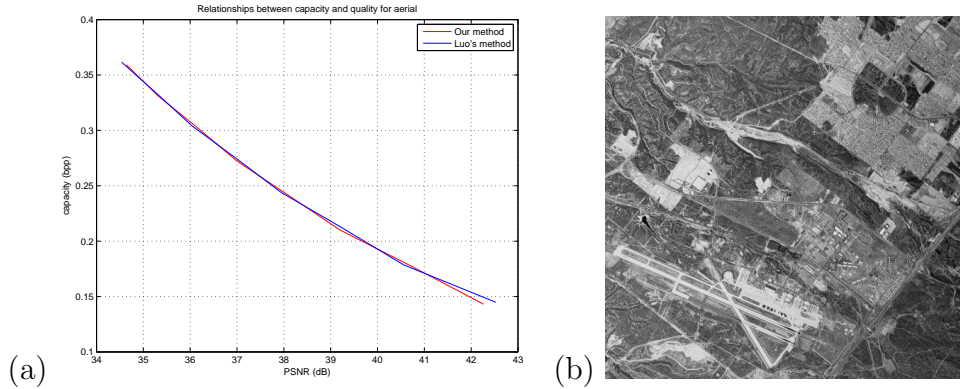


FIGURE 3. Comparisons of (a) objective performances, and (b) subjective quality evaluations for **aerial** when $EL = 18$, with maximal capacity of 0.5291 bpp and PSNR of 31.13 dB.

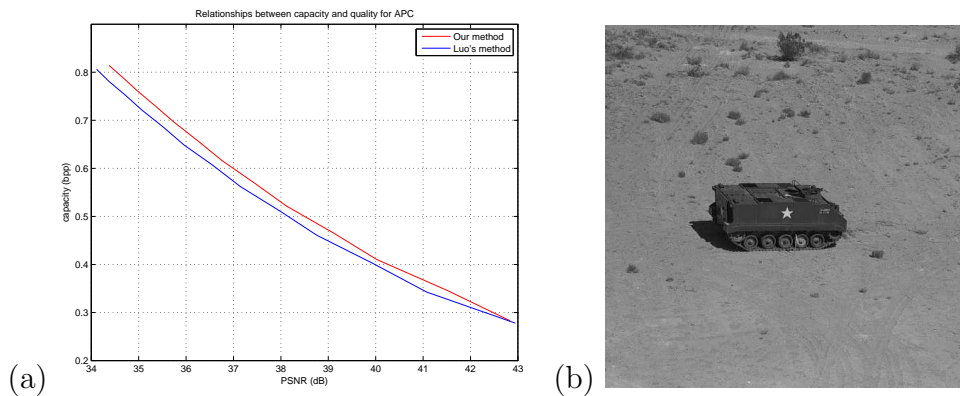


FIGURE 4. Comparisons of (a) objective performances, and (b) subjective quality evaluations for **APC** when $EL = 25$, with maximal capacity of 0.9444 bpp and PSNR of 33.87 dB.

algorithm, both the four parameters and the EL value are needed at the decoder, with the flexibility that the four parameters are adjustable for enhanced performances over [24]. The same amount of side information between our algorithm and that in [24] is observed. For histogram-based scheme [17, 18], only two bytes of side information, denoting the luminance values of peak and zero points, are needed for decoding. With our algorithm, even though slight increase in side information is required, great enhancement in embedding capacity may make up for slight increase in the amount of side information. For DE-based scheme, location map implies a large amount of side information. There is no need to store the location map with our algorithm, and hence less amount of side information is required. Summing up, with our algorithm and in [24], the side information for decoding performs better than conventional histogram- and DE-based schemes.

Comparisons of performances for six test images, listed in alphabetical order, including **aerial**, **APC**, **Barbara**, **F16**, **Goldhill**, and **Lena**, are depicted in Fig. 3 to Fig. 8, respectively. First of all, capability for perfectly separating original image and secret information from marked image, or reversibility of proposed algorithm for the six test images, are verified and guaranteed. With the **aerial** test image, we observe similar performances in Fig. 3(a) between our algorithm, shown in red curve, and those with [24], shown in blue curve. In Fig. 3(b), we demonstrate subjective image quality with the largest embedding

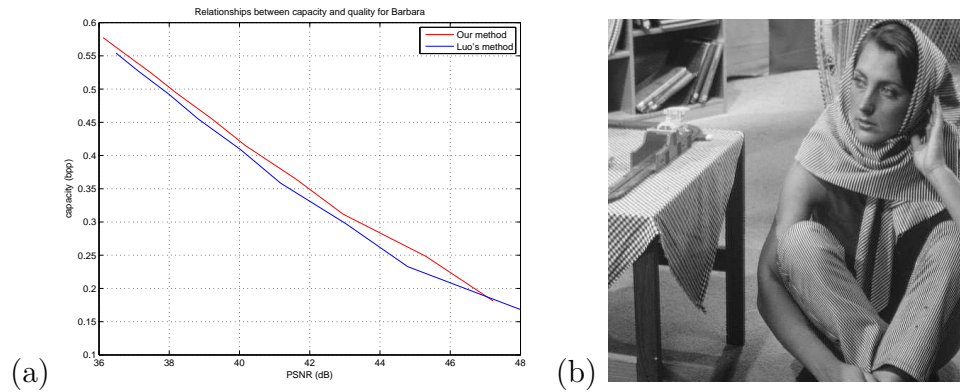


FIGURE 5. Comparisons of (a) objective performances, and (b) subjective quality evaluations for *Barbara* when $EL = 18$, with maximal capacity of 0.6983 bpp and PSNR of 32.93 dB.

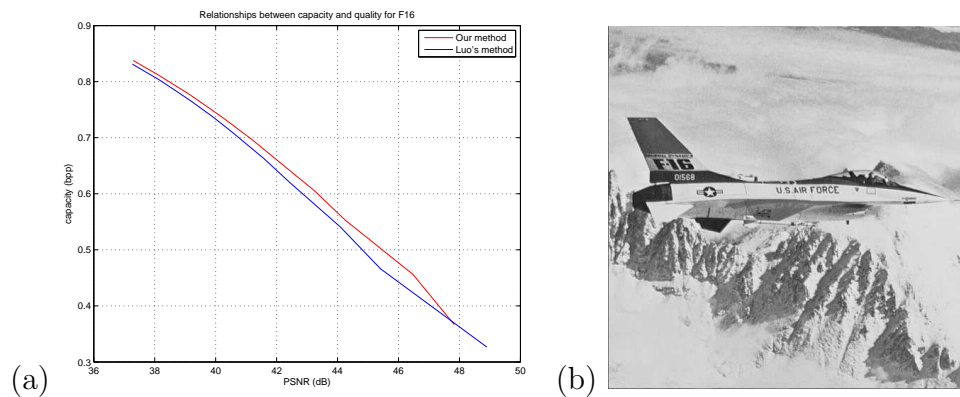


FIGURE 6. Comparisons of (a) objective performances, and (b) subjective quality evaluations for *F16* when $EL = 30$, with maximal capacity of 0.9326 bpp and PSNR of 33.56 dB.

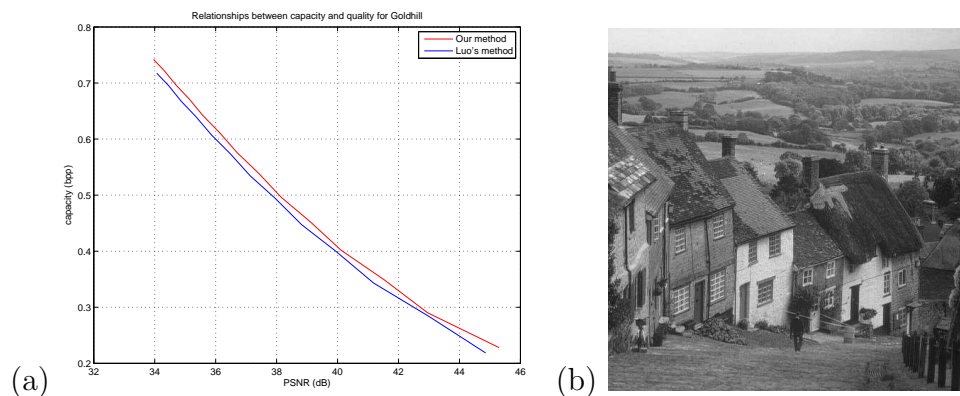


FIGURE 7. Comparisons of (a) objective performances, and (b) subjective quality evaluations for *Goldhill* when $EL = 18$, with maximal capacity of 0.8950 bpp and PSNR of 31.44 dB.

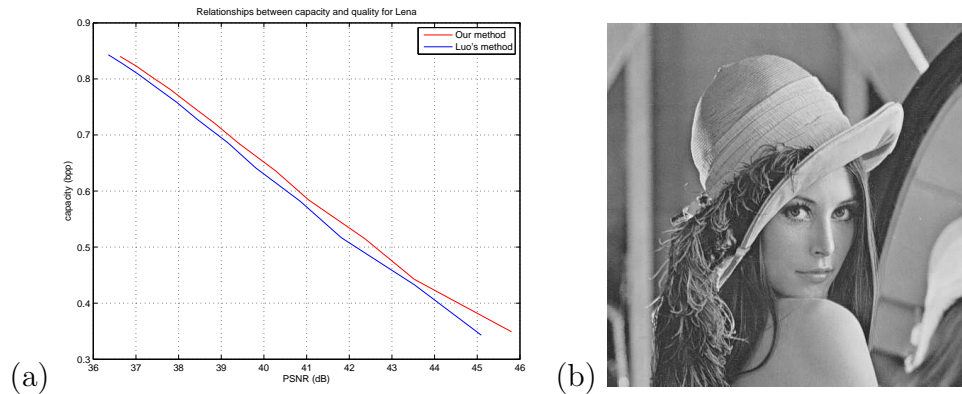


FIGURE 8. Comparisons of (a) objective performances, and (b) subjective quality evaluations for *Lena* when $EL = 25$, with maximal capacity of 0.9347 bpp and PSNR of 34.32 dB.

capacity of 138697 bits, or 0.5291 bpp when $EL = 18$, leading to the PSNR of 31.13 dB. We need to note that with DE-based schemes, capacity may reach at most 0.5 bpp. With proposed algorithm, capacities can easily surpass 0.5 bpp. Finally, we can hardly perceive the embedding of secret data therein, hence the imperceptibility can be retained.

Next, for remaining five test images, subjective evaluations of performances are depicted in Figs. 4(a), 5(a), 6(a), 7(a), and 8(a), respectively. Except for very low embedding capacities in Fig. 5(a), results with our algorithm outperform those with [24] by some margin. With the same amount of capacity, the output image quality in PSNR with our algorithm performs better than those with [24].

In Figs. 4(b), 5(b), 6(b), 7(b), and 8(b), we demonstrate objective image qualities, respectively, with the condition that the maximally allowable capacity for each image is reached. Also, in Table 1, we summarize the experimental results and list the parameters for prediction, the maximally allowable capacity, and corresponding EL and PSNR values for all the six test images. We see that after training the parameters for prediction, enhanced capacity with better image quality can be observed from the simulation results.

Finally, we perform the authentication test for our algorithm. The four values of n_{NW} , n_N , n_{NE} , and n_W can also be served as the secret key for correct decoding and authentication at the decoder. If the four values are received erroneously, even the correct EL value is utilized, after decoding, neither the original image nor the hidden secret would be correctly recoverable. With our algorithm, it is extendable to data authentication algorithm [1], while the algorithm with [24] may have limited flexibility in this application.

Summing up, proposed algorithm performs much better than conventional histogram-based and DE-based schemes in embedding capacity. Considering both the embedding capacity and output image quality, proposed algorithm performs generally better than [24] for images in Figs. 4 to 8, which are able to reside larger capacities, and it performs similar to [24] for images with smaller capacities, such as aerial in Fig. 3. In addition, the four parameters for image prediction can also serve for authentication purposes. Therefore, our algorithm outperforms relating methods in literature.

5. Conclusions. In this paper, we propose an effective algorithm in reversible data hiding by utilizing the prediction of pixel values, and by altering the difference values between predicted image and original one. We aim at obtaining enhanced performances with proposed algorithm. Based on the requirement that predicted image should be as resemble as the original one, weighting factors for prediction should be trained in advance. These

factors can later be served as secret keys for enhanced security. By carefully manipulating differences between predicted and original images, secret data can be embedded by following concepts from conventional histogram-based and DE-based schemes.

Considering the output image quality, the embedding capacity, and the side information for decoding, results with our algorithm generally outperform those with relating algorithms in literature. Similar performances can be reached for low embedding rates, while better performances can be observed for high embedding rates among the six test images. Simulation results have also pointed out performance assessments under a variety of tests. Besides the observations of better image quality, larger embedding capacity, and limited side information, with our algorithm, no calculation is needed for embedding the secret data, which leads to its practical applicability and ease of implementation. Therefore, proposed algorithm is more advantageous over existing ones.

Acknowledgment. This work is supported in part by Ministry of Science and Technology (Taiwan, R.O.C.), under grants MOST103-2221-E-390-018 and MOST104-2221-E-390-012. Authors would like to thank Mr. S. H. Li for part of the programming practices.

REFERENCES

- [1] H. C. Huang and W. C. Fang, "Metadata-based image watermarking for copyright protection," *Simulation Modelling Practice and Theory*, vol. 18, no. 4, pp. 436–445, Apr. 2010.
- [2] B. Yan, Y. Wang, L. Song, H. Yang, "Power spectrum compliant QIM watermarking for autoregressive host signals," *J. Inf. Hiding Multimedia Signal Proc.*, vol. 6, no. 5, pp. 882–888, Sep. 2015.
- [3] H. C. Huang and W. C. Fang, "Authenticity preservation with histogram-based reversible data hiding and quadtree concepts," *Sensors*, vol. 11, no. 10, pp. 9717–9731, Oct. 2011.
- [4] X. Zhang, "Reversible data hiding with optimal value transfer," *IEEE Trans. Multimedia*, vol. 15, no. 2, pp. 316–325, Feb. 2013.
- [5] Y. H. Chen and H. C. Huang, "Coevolutionary genetic watermarking for owner identification," *Neural Computing and Applications*, vol. 26, no. 2, pp. 291–298, Feb. 2015.
- [6] C. C. Lai, H. C. Huang and C. C. Tsai, "Image watermarking scheme using singular value decomposition and micro-genetic algorithm," *Proc. IJHMSP'08*, pp. 469–472, 2008.
- [7] H. C. Huang, F. C. Chang, Y. H. Chen, S. C. Chu, "Survey of bio-inspired computing for information hiding," *J. Inf. Hiding and Multimedia Signal Proc.*, vol. 6, no. 3, pp. 430–443, May 2015.
- [8] J. Marin, F. Y. Shih, "Reversible data hiding techniques using multiple scanning difference value histogram modification," *J. Inf. Hiding and Multimedia Sig. Proc.*, vol. 5, no. 3, pp. 451–460, 2014.
- [9] G. Gao and Y. Q. Shi, "Reversible data hiding using controlled contrast enhancement and integer wavelet transform," *IEEE Signal Processing Letters*, vol. 22, no. 11, pp. 2078–2082, Jul. 2015.
- [10] H. C. Huang, J. S. Pan, W. C. Fang, and L. C. Jain, "An introduction to intelligent multimedia data hiding," *Intelligent Multimedia Data Hiding: New Directions*, Chapter 1, pp. 3–10, 2007.
- [11] Z. Zhao, H. Luo, Z. M. Lu, J. S. Pan, "Reversible data hiding based on multilevel histogram modification and sequential recovery," *AEU-Int'l J. Electron. Commun.*, vol. 65, pp. 814–826, Oct. 2011.
- [12] Y. H. Chen, H. C. Huang, and C. C. Lin, "Block-based reversible data hiding with multi-round estimation and difference alteration," *Multimedia Tools and Applications*, 2015. (DOI: 10.1007/s11042-015-2825-9)
- [13] J. Tian, "Reversible data embedding using a difference expansion," *IEEE Trans. Circuits Syst. Video Technol.*, vol. 13, no. 8, pp. 890–896, Aug. 2003.
- [14] H. Kim, V. Sachnev, Y. Q. Shi, J. Nam, and H. Choo, "A novel difference expansion transform for reversible data embedding," *IEEE Trans. Inf. Forensics Secu.*, vol. 3, no. 3, pp. 456–465, Sep. 2008.
- [15] H. C. Huang and F. C. Chang, "Hierarchy-based reversible data hiding," *Expert Systems with Applications*, vol. 40, no. 1, pp. 34–43, Jan. 2013.
- [16] B. Ou, X. Li, Y. Zhao, R. Ni, Y. Q. Shi, "Pairwise prediction-error expansion for efficient reversible data hiding," *IEEE Trans. Image Processing*, vol. 22, no. 12, pp. 5010–5021, Dec. 2013.
- [17] Z. Ni, Y. Q. Shi, N. Ansari, and W. Su, "Reversible data hiding," *IEEE Trans. Circuits Syst. Video Technol.*, vol. 16, no. 3, pp. 354–362, Mar. 2006.
- [18] X. Li, B. Li, B. Yang, and T. Zeng, "General framework to histogram-shifting-based reversible data hiding," *IEEE Trans. Image Processing*, vol. 22, no. 6, pp. 2181–2191, Jun. 2013.

- [19] H. C. Huang, C. C. Lin, and Y. H. Chen, "Enhancements of reversible data hiding by interpolation-based prediction with difference alteration," *Proc. IHHMSP'15*, pp. 147–150, 2015.
- [20] X. Li, W. Zhang, X. Gui, and B. Yang, "A novel reversible data hiding scheme based on two-dimensional difference-histogram modification," *IEEE Trans. Information Forensics and Security*, vol. 8, no. 7, pp. 1091–1100, Jul. 2013.
- [21] C. S. Shieh, H. C. Huang, T. Y. Chen, and J. S. Pan, "BTC-immunized watermarking using local homogeneity for pixel selection," *Proc. KES'02*, pp. 422–426, 2002.
- [22] H. C. Huang and W. C. Fang, "Reversible data hiding using characteristics of original contents," *Proc. Int'l Conf. Security and Management*, pp. 426–432, 2010.
- [23] H. Hu, H. K. Lee, and J. Li, "DE-based reversible data hiding with improved overflow location map," *IEEE Trans. Circuits Syst. Video Technol.*, vol. 19, no. 2, pp. 250–260, Feb. 2009.
- [24] H. Luo, F. X. Yu, Z. L. Huang, H. Chen, and Z. M. Lu, , "Reversible data hiding based on hybrid prediction and interleaving histogram modification with single seed pixel recovery," *Signal, Image and Video Processing*, vol. 8, no. 5, pp. 813–818, Jul. 2014.